Modeling of H2/air flame stabilization regime above coaxial dual swirl injectors

S. Marragou, Hervé Magnes, A. Aniello, T.F. Guiberti, L. Selle, Thierry Poinsot, Thierry Schuller

Modeling of H_2/air flame stabilization regime above coaxial dual swirl injectors

S. Marragou[a,*], H. Magnes[a], A. Aniello[a], T. F. Guiberti[b], L. Selle[a], T. Poinsot[a], T. Schuller[a]

[a] *Institut de Mécanique des Fluides de Toulouse, IMFT, Université de Toulouse, CNRS, Toulouse, France*
[b] *Physical Science and Engineering Division, Clean Combustion Research Center, King Abdullah University of Science and Technology, Thuwal, 23955, Saudi Arabia*

Abstract

The prediction of the stabilization regime of partially premixed H_2/air flames above an injector is a main subject of interest for the development of gas turbines powered by hydrogen. The way the flame is stabilized has an impact on NOx emissions, thermal stress on the injector, and combustion stability. A model based on the triple flame speed is revisited and improved to predict flame stabilization using information gathered at cold flow conditions. The model is called TFUP for Triple Flame Upstream Propagation. According to this model, the flame can anchor to the injector only if a zone with a flammable mixture and a sufficiently low local flow velocity exists continuously from the lifted flame to the injector lips. The TFUP model is applied to the case of a H_2/air coaxial, dual swirl injector in which both the hydrogen and air streams are swirled. Fuel is injected through the central channel and oxidizer through the external channel. Particle image velocimetry and one dimensional Raman scattering measurements made at strategic locations are used to predict the edge flame speed for which a lifted flame should re-anchor to the injector. These predictions made in isothermal conditions are compared to observations of the flame stabilization regime. The central flow of hydrogen can be mixed with methane and helium and the external flow of air with nitrogen in order to prescribe different theoretical values for the triple flame speed. Predictions agree well with the observations made for all swirl levels conferred to the central fuel stream, fuel injection velocities, hydrogen contents in the fuel mixture injected in the central channel, and nitrogen contents in the oxidizer annular channel tested in the study. Validity limits are also discussed. The methodology presented in this study provides a simple framework to predict flame stabilization on coaxial injectors that can optionally be equipped with swirl vanes.

Keywords:
Flame stabilization, Hydrogen combustion, Swirled burner, Coaxial injector, Lifted flame, Gas turbine

*Corresponding author: sylvain.marragou@imft.fr

1. Introduction

Substitution of hydrocarbon fuels with hydrogen produced from renewable resources in gas turbines can be used to decarbonize power production [1], and is also considered to decarbonize aviation [2]. However the transition to hydrogen raises many technological issues. Due to its high reactivity, combustors operating with hydrogen are more prone to flashback, to higher NOx emissions and to higher thermal stress on solid walls than systems powered by standard hydrocarbon fuels [3, 4].

The increased propensity to flashback with hydrogen admixtures is due to its reactivity [5, 6] limiting the burner operability. Injection of hydrogen separately from the oxidizer avoids the flashback risk, but the resulting diffusion flames lead to high local temperatures producing unacceptable NOx emission levels [3, 5]. In the last decades, new hydrogen combustor architectures have been developed to manage flashback risks and mitigate NOx emissions. They generally consist of radially injecting small jets of hydrogen into the oxidizer stream a few centimeters upstream of the outlet of the oxidizer channel [7, 8]. These disruptive technologies require large modifications of the combustion chamber architecture compared to current systems in which combustion is stabilized by using a swirling flow.

An alternative solution has recently been investigated in [9, 10] with a coaxial dual swirl injector, where hydrogen is injected through a central tube with a swirled vane and the oxidizer stream is also swirled inside the annular channel. The injector is designed to work with hydrogen as fuel and air as oxidizer, but it can also be operated with mixtures of different combustibles and inert gases. Moreover, air can be diluted with nitrogen. Flashback is avoided by the late introduction of hydrogen within the oxidizer stream. Experiments at atmospheric conditions indicate that NOx emissions remain controlled when the flame is lifted above the injector and that swirling the central hydrogen stream favors its fast mixing with air before reaction [10]. As a positive side effect, lifted flames, detached from all solid components of the combustor, limit also the thermal stress on the injector.

In a coaxial injector, conferring a swirl motion to the annular oxidizer stream is a standard method to create a central recirculation zone (CRZ) and to obtain aerodynamically stabilized flames over a wide range of operating conditions [11]. However in most gaseous fuel and air coaxial injection systems, only the oxidizer stream is swirled [12, 13]. Yuasa [14] observed that conferring swirl to a central fuel lance in an annular labscale unconfined burner substantially helped lifting methane flames from the central fuel nozzle. Nevertheless, when methane was replaced with hydrogen, the flame remained anchored to the fuel nozzle over the entire range of hydrogen injection velocities explored, even when hydrogen was injected close to sonic conditions. Degeneve *et al.* [15, 16] investigated the stabilization of methane oxy-flames in which both the methane, injected through a central lance, and the oxidizer stream, injected through an annular channel, were swirled. They observed that swirling the central fuel stream greatly helped flame lifting above the injector lips despite the strong reactivity and resistance to strain rate of these flames. Similar coaxial injection systems adopting swirlers either in fuel and oxidizer channels were recently investigated to analyze the resulting hydrogen/air flame topologies [9, 10, 17]. It was shown in [9, 10] that slightly shifting the hydrogen lance nozzle in the upstream direction with respect to the annular air stream nozzle outlet drastically improves the burner operability with lifted hydrogen/air flames. Mixing between two coaxial swirled streams was also recently characterized by Raman scattering in a study where the recess of the central lance was adjusted in order to mitigate combustion instabilities [18].

In these studies, the impulsion ratio $J = \rho_e u_e^2 / \left(\rho_i u_i^2\right)$ between the external and internal streams is a key parameter controlling flame lift-off as for non-swirling coaxial injectors [19]. Nevertheless, it was shown in [9] that the hydrogen injection velocity u_i in the central channel is more important than the impulsion ratio J to analyze the observed flame transitions. The offset distance between the two nozzles studied in [10] is also important to consider. This offset was also shown to be critical for swirled coaxial liquid rocket injectors [20, 21]. Finally, the swirl level S_e in the annular oxidizer stream and the swirl level S_i in the central fuel stream were also shown to alter the flow topology and flame stabilization [10, 16]. Still, the detailed mechanisms by which the flame is anchored or lifted from the fuel injector remain to be elucidated for these dual swirled coaxial injectors.

The knowledge gained on the stabilization of jet flames above non-swirling coaxial injectors can be used as a starting point. Several physics based models have been proposed to explain the stabilization of lifted turbulent flames that were reviewed in [22]. Vanquickenborne and van Tiggelen [23] argued that for lifted flames, the fuel and oxidizer streams mix before ignition and the flame stabilizes on the stoichiometric line where the local flow velocity is equal to the turbulent flame

speed. Another explored hypothesis is that the stabilization of lifted turbulent flames results from local flame extinction due to the quenching of laminar flamelets when the local value of the non-dimentionalized scalar dissipation rate falls below a critical threshold [24]. According to Byggstøyl and Magnussen [25], stabilization is controlled by local flame extinction at the smallest turbulence scales. Since 20 years, a consensus has however been reached about the mechanisms leading to flame re-anchoring. The beginning of the lifted reaction zone is seen as an edge flame that propagates against the flow along the stoichiometric line [26] to reach a stabilization point, typically located at the injector lips [27].

Edge flames were extensively studied [28] and can be assimilated in certain cases to an idealized triple flame [29, 30]. Muñiz and Mungal [31] revisited the Vanquickenborne and van Tiggelen [23] model considering the leading-edge flame speed instead of the turbulent flame speed. In their experiments, they found that the leading-edge reaction front of the lifted flame can propagate towards the injector lip if the local velocity along the stoichiometric line connecting the flame to the injector is lower than the triple flame speed. They concluded that leading-edge flames, which have similar characteristics as triple flames, are more consistent to describe flame re-anchoring than any models based on a turbulent flame speed.

Ruetsch *et al.* [32] derived a relation that account for heat release rate effect to estimate the theoretical value of the propagation speed of a triple flame. Cha and Ronney [29] measured the propagation speed of non-premixed edge flames for different fuels and different oxidizer dilutions and found that the relation proposed in [32] corresponds for most cases to the maximum displacement speed reached by edge flames, except for CO_2 diluted mixtures. In the model [32], the correction $(\rho_u/\rho_b)^{1/2}$ originates from the modification of the flow field by the edge flame structure. The curved flame decelerates the flow in front of the flame due to momentum and mass balances across the curved edge flame reaction layer leading to a higher flame displacement speed than the laminar burning velocity s_L relative to the flow unaffected by the flame [33].

Further experiments have been conducted to unveil the different stabilization regimes of turbulent flames above coaxial injectors. These studies are generally carried out with a small air co-flow and without swirl. Brown *et al.* [34] concluded that the velocity of the leading edge of a lifted flame is in most cases bounded by $3s_L$, where s_L is the laminar burning velocity of a stoichiometric mixture. But for some cases, they observed that this local velocity better scales with a turbulent burning velocity s_T. Joedicke *et al.* [35] confirmed these observations for hydrocarbon lifted flames and highlighted the triple flame structure of the leading edge front in their experiments. They also showed that the flame leading edge does not exactly coincide with the location of the stoichiometric line, but preferentially lies at $Z \simeq 1.1Z_{st}$, where Z is the mixture fraction passive scalar and Z_{st} its stoichiometric value. Guiberti *et al.* [36] confirmed these observations using advanced laser diagnostics varying the pressure inside the combustion chamber. They identified two regimes. For unperfect mixing of fuel and oxidizer streams, the stoichiometric line is present at the axial location of the flame base and the local flow velocity of the leading edge of the lifted flame is slightly above $3s_L$. When premixing of the oxidizer and fuel streams is sufficiently advanced, this line does not exist anymore and combustion takes place in premixed conditions. In this latter case, the local velocity of the leading edge front is roughly equal to s_T, a turbulent flame speed estimated from empirical correlations. This last regime is observed above a critical value of the air co-flow velocity in their setup.

In the first regime, when a thin stoichiometric line separates fuel and air on both sides, the Muñiz and Mungal [31] scenario was recently considered in [10] to explain the transitions from lifted to attached flames observed for the dual swirl hydrogen/air injector studied in [9]. A Triple Flame Upstream Propagation (TFUP) zone was defined around the hydrogen nozzle lip with boundaries delineating the positions where the local flow velocity corresponds to the triple flame speed as defined in [32]. It was hypothesized that when the stoichiometric mixture fraction line intersects the TFUP zone, a lifted flame is able to re-anchor to the fuel nozzle. This model was corroborated by two sets of experiments in which the hydrogen and air streams were diluted leading either to a change of the triple flame speed, the location of the stoichiometric mixture fraction being unchanged or to a change of the position of the stoichiometric mixture fraction line with respect to the TFUP boundary, the triple flame speed being unchanged. Observations confirmed the TFUP model predictions, but direct quantitative validations could not be achieved because the velocity and mixture fraction fields could not be determined in [10] due to the limited optical access to the outlet of the burner.

The first objective of this study is to revisit and improve the TFUP model presented in [10]. The second one is to validate it on a quantitative basis by detailed comparisons between predictions and experiments for a wide range of conditions leading to flame re-anchoring.

The last objective is to develop a relatively simple way of predicting H_2/air flame stabilization regimes above non premixed swirled injectors using only a limited set of experiments or simulations carried out in cold flow conditions. The main novelty of the TFUP zone model is to take both the axial and radial velocity components of the flow field into consideration for the delineation of the zone around the lips of an injector through which an edge flame can propagate. It will be shown that determining the boundaries of the TFUP zone for a given couple of fuel and oxidizer enables to infer the operating conditions leading to flame re-anchorings on the fuel nozzle.

The experimental setup and the diagnostics are presented in Section 2. The different flame stabilization regimes are described in Section 3. The improved TFUP model used to predict the flame stabilization regime is described in Section 4. It relies on the determination of the angle of the line along which edge flames can propagate. This procedure is described in Section 5. Results for the TFUP model and comparisons with measurements are then presented in Section 6.

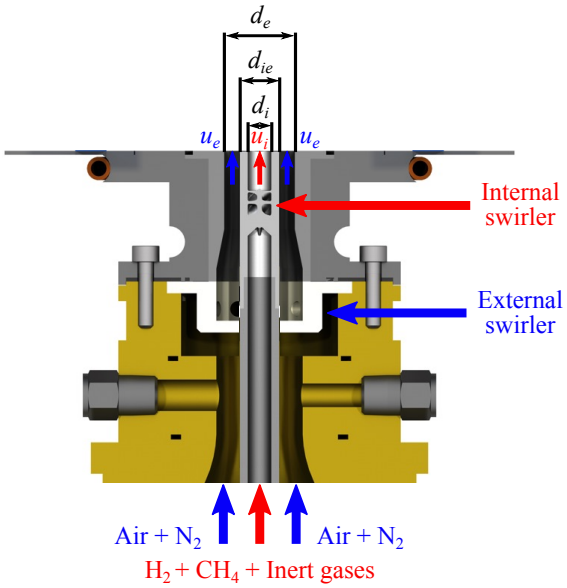

Figure 1: MIRADAS test rig equipped with the HYLON injector. In all experiments, the fuel and oxidizer channels are flush mounted with the combustion chamber backplane.

2. Experimental setup

Experiments are conducted with the MIRADAS test bench [37] equipped with the HYdrogen LOw NOx (HYLON) injector [9, 10]. HYLON is a dual swirl coaxial injector described in Fig. 1. The burner can be powered by methane and hydrogen. Air and various diluents including nitrogen, argon and helium can also be injected in the fuel or oxidizer streams. All flow rates are regulated with mass flow controllers (Brooks SLA 585x series and Bronkhorst F201-AV-x series). The bottom part of the burner consists of a plenum fed by the oxidizer, air possibly diluted with nitrogen, a convergent, and an annular channel that is equipped with a radial swirler. The swirled oxidizer then flows through an external annular channel outlet with an outer diameter d_e = 18 mm and an inner diameter d_{ie} = 10 mm that corresponds to the external diameter of the central hydrogen injector. All experiments presented in this study are conducted for a fixed external swirl number S_e = 0.67.

The fuel is injected through a central tube of inner diameter d_i = 6 mm equipped with an axial swirl vane. Different swirl vanes can be used to vary the swirl number S_i from 0.0 to 0.9. The fuel can be pure hydrogen or a mixture of hydrogen and methane possibly diluted with argon or helium. For experiments conducted in cold flow conditions, hydrogen is replaced by helium. In this study, the oxidizer and fuel channels are flush mounted with the combustion chamber backplane to provide a full optical access to the HYLON burner lips and unlike [9, 10] enable to scrutinize the flow with laser diagnostics. The central and annular jets exhausting from the coaxial injector expand in a combustion chamber with a square cross section of 78 mm width equipped with four quartz windows. A nozzle is installed at the top of the combustion chamber with a cross section area contraction ratio of 0.69 and a circular outlet to avoid ambient air entrainement inside of the combustor.

A Particle Image Velocimetry (PIV) system is installed as shown in Fig. 2a to characterize the velocity field in the axial plane close to the burner outlet. The velocity field is determined for cold flow conditions, where hydrogen is replaced by the same volumetric flowrate of helium. The choice was made to keep the same injection velocity as for hydrogen in order to limit the alteration of the hydrodynamic flow field in the vicinity of the central jet as explained in [10]. Seeding in the external and internal injection channels is achieved with small mineral oil droplets atomized with commercial perfume nebulizers. The laser is a double head Quantel Big Sky Laser CFR200 and the light scattered by the oil droplets is recorded with a PCO.2000 2048×2048 pixels camera equipped with a Nikkor 105 mm f/2.8G lens. Synchronization between the laser and the camera is made with an homemade electronic system. The delay between images in a pair

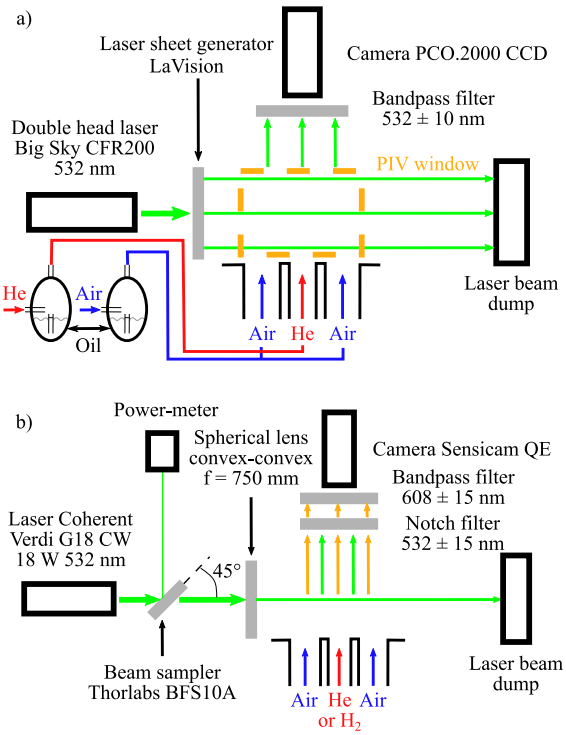

Figure 2: Schematic of the optical diagnostic systems used in this study: (a) Particle Image Velocimetry (PIV) system. (b) 1D1S Raman scattering system.

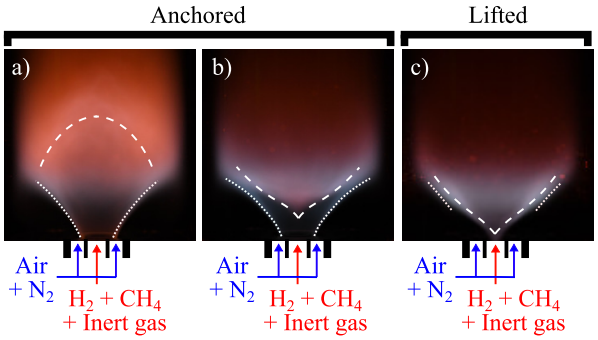

Figure 3: Flame archetypes observed with the HYLON injector. (a) Attached flame for $S_i = 0$. (b) Attached flame with $S_i > 0$. (c) Lifted flame with $S_i > 0$. Dotted lines: shear layer stabilized flame. Dashed lines: central reaction layer. Flame images are recorded in the visible spectrum.

is set to 3 μs. Velocity vectors are determined from 32×32 pixels interrogation windows with an overlap of 75%. This setup yields a 20×20 mm field of measurements with a vector resolution of 78 μm in each direction. All measurements are the result of an average over 500 snapshots sampled at 10 Hz leading to a statistically converged information for the mean velocity in the central axial plane of the burner.

Flame images are recorded with an intensified Princeton Instrument PI-MAX 4 camera equipped with a Nikon UV-105, 105 mm f/4.5, Rayfact Multispectral lens and a 10 nm bandpass filter centered on $\lambda = 310$ nm Asahi XHQA310. This camera is used to collect the OH^* chemiluminescence from the flame and deduce the location of the heat release [38].

Raman scattering in the cold flow is also used to analyze mixing between the oxidizer and fuel streams with the optical setup shown in Fig. 2b. It comprises a continuous Coherent Verdi G18 laser producing a p-polarized laser beam at $\lambda = 532$ nm. A part of the laser beam is deviated with a Thorlabs BFS10-A beam sampler to a Thorlabs S425C power meter to monitor the stability of the laser source. The beam is focused in the center of the combustion chamber using a convex-convex spherical lens of 750 mm focal length. The luminosity of the laser beam, laser reflections and the Rayleigh scattered light are filtered out by a Edmund Optics 532±15 nm OD4 notch optical filter. The remaining scattered light is filtered around 605 nm with an OD4 Edmund Optics 86367 15 nm bandpass filter. This optical system enables to record the light scattered by the N_2 molecules within air by Raman anti-stokes effect around 607 nm. Images of this signal are collected with a PCO Sensicam QE camera equipped with a Nikkor 105 mm f/2.8G lens. Calibrations are made with a set of pure gases before each measurement to deduce the relation between the light intensity and N_2 molar fraction. These data are used to deduce the mixture fraction. Measurements are first conducted with hydrogen injected in the central lance and air and compared to measurements when hydrogen is replaced with helium. As for the PIV measurements, the hydrogen flow in the central tube is for most experiments conducted in cold flow conditions replaced by the same volumetric flowrate of helium.

3. Flame stabilization regimes

Three different flame archetypes illustrated in Fig. 3 can be observed with HYLON. Without swirl in the central injection tube ($S_i = 0.0$), the flame is always anchored to the central injector lip as in Fig. 3a. This flame is characterized by two different diffusion reaction layers. The reaction delineated by the dotted lines is a diffusion front. Reaction takes place at stoichiometry in the shear layer between the oxidizer external stream and the central fuel stream. A second weaker diffusion reaction layer delimited by dashed lines in Fig. 3a is

stabilized between hot vitiated gases recirculating in the Central Recirculation Zone (CRZ) and the central hydrogen jet penetrating into the CRZ as confirmed by the numerical flow simulations conducted in [39]. Combustion of hydrogen with vitiated hot gases explains the reddish color around this reaction layer due to the chemiluminescence of highly vibrational excited H_2O molecules that takes place in very hot zones [40]. Two other flame archetypes are observed when the central hydrogen lance is equipped with a swirler ($S_i > 0$).

The second flame archetype, shown in Fig. 3b, is similar to that shown in Fig. 3a and corresponds also to a flame anchored to the central tube nozzle. The only difference is the shape of the central reaction front delimited by dashed lines that takes now a V-shape in Fig. 3b. The pale blue/gray color of the external flame front delimited by dotted lines is attributed to the chemiluminescence of excited H_2O_2 radicals [41]. When swirl is conferred to the central hydrogen stream, the hydrogen jet expands radially -as shown in [10]. As a consequence, the central jet does not penetrate anymore deeply inside of the CRZ like it does for the non-swirling hydrogen jet case in Fig. 3a, and the curvature of the central reaction layer is now reversed in Fig. 3b compared to Fig. 3a.

The third flame archetype shown in Fig. 3c corresponds to a lifted flame. This aerodynamically stabilized flame is detached from all solid components of the injector and stays away from the combustor walls. The distance between the fuel injector outlet and the flame as well as the fast radial expansion of the central swirling jet lead to a fast mixing between the oxidizer and the fuel streams before reaction. The resulting flame burns in a partially premixed regime [39] and takes a V-shape delimited by the dashed lines in Fig. 3c. For some operating conditions, two additional branches, represented in Fig. 3c by the dotted white lines, appear in the external shear layer close to the main flame reaction layer. When these additional branches approach too close to the central injector lips, the flame stabilization regime suddenly switches to a re-anchored flame, i.e. a flame attached to the central injector. This sharp bifurcation from lifted to re-anchored flame takes place systematically for the same operating conditions.

4. Triple Flame Upstream Propagation (TFUP) zone model

Previous experiments [9, 10] revealed that the stabilization regime, anchored or lifted, mainly depends on the swirl numbers S_e and S_i in both injection channels, the central injector recess distance, and the central injection velocity u_i. It was also shown that flames are more easily lifted when methane is added in the external oxidizer channel. A transition model for lifted to re-attached flame has been introduced in [10], which is revisited below and improved.

The flow is considered as two dimensional in the following analysis. The azimuthal velocity component of the swirling flow is discarded. It will be shown that the effect of swirl on flame stabilization can be captured by only considering the radial component of the velocity field. It is also hypothesized that the velocity field close to the burner outlet remains unchanged in cold and hot conditions when the flame is lifted, i.e. the burnt gas expansion taking place downstream of the flame front does not affect the flow velocity field between the central injector lips and the flame. Following Muñiz and Mungal [31], an edge flame can anchor to the central injector lips separating the fuel from the oxidizer only if its leading edge displacement speed s_d is higher than the local flow velocity along the stoichiometric mixture fraction line Z_{st}. In [10], the maximum propagation speed of an edge flame s_d is assumed to match the triple flame speed [32]. This hypothesis is corroborated by measurements of the edge flame velocity carried out by Cha *et al.* [29].

However, as already noticed in [31, 35], an edge flame propagates along the mixture fraction line Z_m for which its displacement speed s_d is maximum. This mixture fraction line is close to stoichiometry for most of hydrocarbon fuels, such as methane, but can be higher for other fuels. In case of hydrogen for instance, the equivalence ratio leading to the maximum displacement speed s_d is equal to $\phi_m = 1.65$. If this mixture fraction does not exist between the flame and the injector lip, the edge flame will propagate along a mixture fraction line corresponding to a lower fuel concentration.

To summarize, a lifted flame can move upstream only if two conditions are met: (i) a flammable mixture fraction line Z_0 between the flame and the injector rim exists and (ii) the mixture fraction line Z_0 is located, from the flame to the injector lip, in a zone where the projection of the local flow velocity along this line $u_t = \mathbf{u} \cdot \mathbf{t}$, i.e. the flow velocity seen by the edge flame, is lower than its propagation velocity s_d. Foley *et al.* [42] already noticed that the local flow velocity at the leading edge flame should be projected tangentially to the flame propagation direction. In Fig. 4, the unit vector $\mathbf{t}$ is tangent to the Z_m iso-level, i.e. to the propagation direction of the edge flame. Condition (ii) delineates the boundary of the Triple Flame Upstream Propagation (TFUP) zone:

$$u_t \leq s_d \tag{1}$$

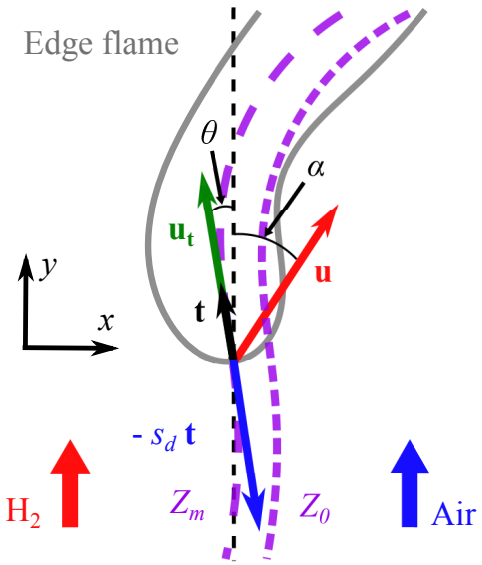

Figure 4: Schematic of an edge flame propagating along the Z_m mixture fraction line with the notations used to determine the boundaries of the TFUP zone.

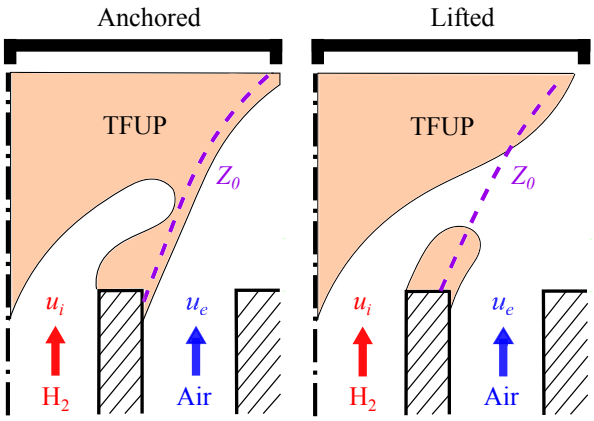

Figure 5: Representation of the TFUP model for (a) an anchored flame and (b) a lifted flame. The edge flame propagation line Z_0 is drawn in purple dashed lines and the TFUP zone is colored in orange.

To take these features into account the displacement speed model used in [10] is slightly modified. The edge flame speed s_d along the mixture fraction line Z_0 is here estimated as follows:

$$s_d = s_L^0 \left(\frac{\rho_u}{\rho_b}\right)^{1/2} \tag{2}$$

where s_L^0 is the laminar burning velocity reached for Z_0 and ρ_u/ρ_b the volumetric expansion ratio of the gas through the flame calculated for Z_0. The mixture fraction Z_0 is in most cases equal to Z_m associated to the maximum laminar burning velocity s_L^m and maximum triple flame speed, when the mixture fraction Z_m is reached within the TFUP zone. If only leaner mixture fractions than Z_m are reached within the TFUP zone boundaries, the edge flame propagates along the Z_0 mixture fraction line featuring the highest triple flame speed.

Notations used for vector projections are introduced in Fig. 4. The angle θ of the flame propagation line Z_0 and the angle α of the local flow velocity with respect to the vertical axis are determined in the following experiments to get the local velocity $u_t = \mathbf{u} \cdot \mathbf{t}$ tangent to the Z_0 line:

$$u_t = u \cos(\alpha - \theta) \tag{3}$$

where u is the modulus of the flow velocity in the axial plane of the burner. With these notations, the condition Eq. (1) for flame re-anchoring becomes:

$$u \cos(\alpha - \theta) \leq s_L^0 (\rho_u/\rho_b)^{1/2} \tag{4}$$

Figure 5 shows the two possible cases. In this diagram, the flame propagation line Z_0 corresponds to the purple dashed lines. To propagate towards the hydrogen nozzle rim, the edge flame needs to overcome the velocity $u_t = \mathbf{u} \cdot \mathbf{t}$ of the local flow along the Z_0 line. The TFUP zone where the flame can propagate upstream is colored in orange. When the Z_0 line intersects the TFUP zone, the flame re-anchors as in Fig. 5a. If the TFUP zone is disrupted near the nozzle lip, the flame remains lifted as in Fig. 5b.

Values for ρ_u, ρ_b and s_L^0 at Z_0 are determined with Cantera for adiabatic freely propagating one dimensional premixed flames at ambient conditions with the San Diego kinetic mechanism [43]. For a H_2/air flame, the laminar burning velocity reaches his maximum $s_L^0 = s_L^m = 3.17$ m/s and $\rho_u/\rho_b = 6.37$ for $Z_0 = Z_m = 0.046$. Equation (2) yields in this case a displacement speed equal to $s_d = 7.99$ m/s.

In the following, the position of the Z_0 line is deduced in the following from OH^* flame images and Raman scattering data while the local flow velocity is inferred from PIV measurements.

5. Experimental determination of TFUP zone

A set of experiments is carried out to test the ability of the TFUP model to predict the transition from lifted to anchored flame. Measurements are conducted for three target flow configurations F_x with $x = 1$, 2 or 3 as described in Table 1. The bulk flow velocity $u_e = 28.5$ m/s

Table 1: Flow conditions with corresponding injection velocities u_e and u_i. The velocities are calculated for standard inlet gas conditions at T_0=20°C and p_0=1 atm

Flow conditions	u_e [m/s]	u_i [m/s]
F_1	28.5	17.0
F_2	28.5	34.0
F_3	28.5	45.0

and the swirl level $S_e = 0.67$ in the external annular channel are fixed. The bulk velocity u_i in the internal channel can be fixed to $u_i = 17$ m/s for F_1, $u_i = 34$ m/s for F_2 or $u_i = 45$ m/s for F_3. To modify the flow field near the injector outlet, the swirl level in the internal fuel channel is varied from $S_i = 0.0$ to 0.9. The following notation is introduced to identify the cases which are considered $F_x - S_i - O/F$, where F_x denotes the couple of injection velocities that are tested, S_i is the swirl level in the internal channel, O designates the oxidizer gas mixture injected in the annular external channel and N the fuel gas mixture injected in the central channel. To modify the location of the stoichiometric mixture fraction line, the injection scheme $F_x - S_i - Air/H_2 + Ar$ is used, with air injected in the annular channel and H_2 eventually diluted with argon injected in the central channel. To modify the triple flame speed, the injection scheme $F_x - S_i - Air/H_2 + N_2 + CH_4 + He$ is adopted. These experiments are conducted for fixed bulk flow injection conditions while the fuel-oxidizer composition is changed in each channel.

An estimation of the local angle θ in Fig. 4 of the edge flame propagation line with respect to the vertical axis is needed to deduce the TFUP boundaries from PIV measurements. Without the possibility to measure directly the location of this line with a sufficient spatial resolution, its position is inferred from attached flames by detecting the flame front position. It has been verified with high fidelity simulations [39] that the diffusion branches from the base to the top of anchored flames correspond roughly to the location of the stoichiometric mixture fraction Z_{st} line. The angle between the Z_{st} line and the vertical axis is here assumed to be approximately the same as the angle of the edge flame propagation line, even though this line does not necessarily coincide with the stoichiometric mixture fraction line.

A sensitivity analysis is first conducted to compare the angles with the vertical axis deduced for different mixture fractions and analyze their impact on the boundary of the TFUP zone. Flame images are recorded and an Abel deconvolution is applied to infer the OH^* distribution in the symmetry plane of the burner. The lo-

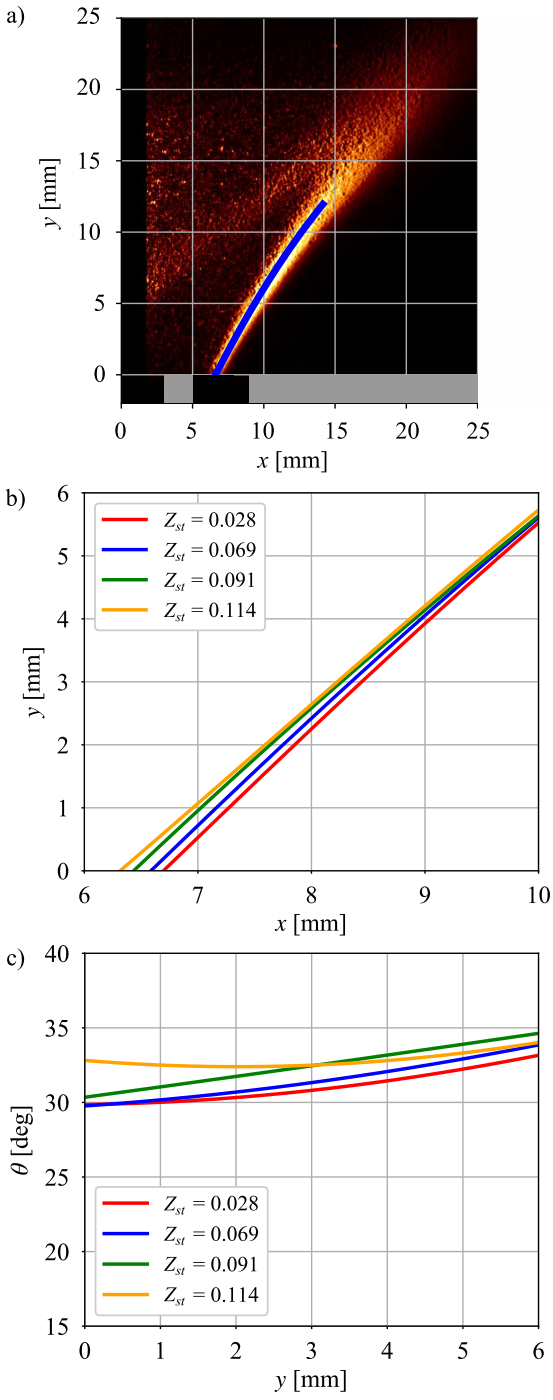

Figure 6: Illustration of the methodology used to infer the angle θ for case $F_2 - 0.9 - Air/H_2 + Ar$ (see Table 1). (a) Abel deconvoluted OH^* image with the detected flame front superimposed in blue. (b) Detected flame front locations and (c) flame angle θ with the vertical axis for different values of the stoichiometric mixture fraction Z_{st} of diluted $Air/H_2 + Ar$ mixtures described in Table 2.

Table 2: Diluted flames with argon mass fraction Y_{Ar} in the hydrogen lance for cases $F_2 - S_i - Air/H_2 + Ar$ (see Table 1 for flow conditions): thermal power P, equivalence ratio ϕ, stoichiometric mixture fraction Z_{st}, and mixture fraction Z_m corresponding to the equivalence at which the laminar burning velocity is maximum.

Y_{Ar}	P [kW]	ϕ	Z_{st}	Z_m
0.00	9.7	0.46	0.028	0.046
0.61	9.0	0.43	0.069	0.114
0.71	8.6	0.41	0.091	0.150
0.77	8.3	0.40	0.114	0.188

cation of the flame front is deduced from the maximum of OH^* intensity. The case $F_2 - S_i - Air/H_2 + Ar$ is considered for this purpose with results shown in Fig. 6. Figure 6a shows the detected flame front in blue which is superposed to the Abel deconvoluted OH^* image. To mimic the impact of various levels of the mixture fraction, these experiments are repeated when hydrogen is diluted with argon in the central lance as summarized in Table 2. Argon is chosen because of his large molar weight with respect to hydrogen. A small volumetric concentration of argon in the fuel substantially increases the value of the stoichiometric mixture fraction Z_{st} but barely alters the bulk flow injection velocity u_i inside the central lance. The position of the detected flame front is plotted in Fig. 6b for mixture fractions spanning from $Z_{st} = 0.028$, i.e. when pure hydrogen is injected, to $Z_{st} = 0.114$ for hydrogen diluted with $Y_{Ar} = 0.77$. As a consequence, the flame position corresponding to the OH^* peak intensity slightly moves towards the burner center in Fig. 6b as predicted by theory. The angles θ deduced from these plots are presented in Fig. 6c. Figures 6b-c show that despite the differences observed in Fig. 6b for the mixture fraction lines when Z_{st} is varied, their impact on θ in Fig. 6c remains limited. The difference is less than 3° between all cases over the first 6 mm above the burner.

The impact of the chosen angle θ determined for different mixture fractions Z_{st} on the boundary of the TFUP is now assessed with the help of Eq. (4). Information on the velocity field, i.e. u and α, is determined from PIV data and the edge flame speed $s_d = s_L^0(\rho_u/\rho_b)^{1/2}$ with Cantera as described in the previous section. In order to highlight only the influence of the angle θ, the value of $s_d = 7.99$ m/s is fixed to the maximum triple flame displacement speed of an hydrogen/air flame. The location of the TFUP zone is presented in Fig. 7 as a function of the mixture fraction selected to determine its boundary. Results are illustrated for an inert flow with helium injected in the central lance. Despite the large variation of the theoretical value of Z_0 spanning from 0.028 to 0.114 used to infer the angle θ,

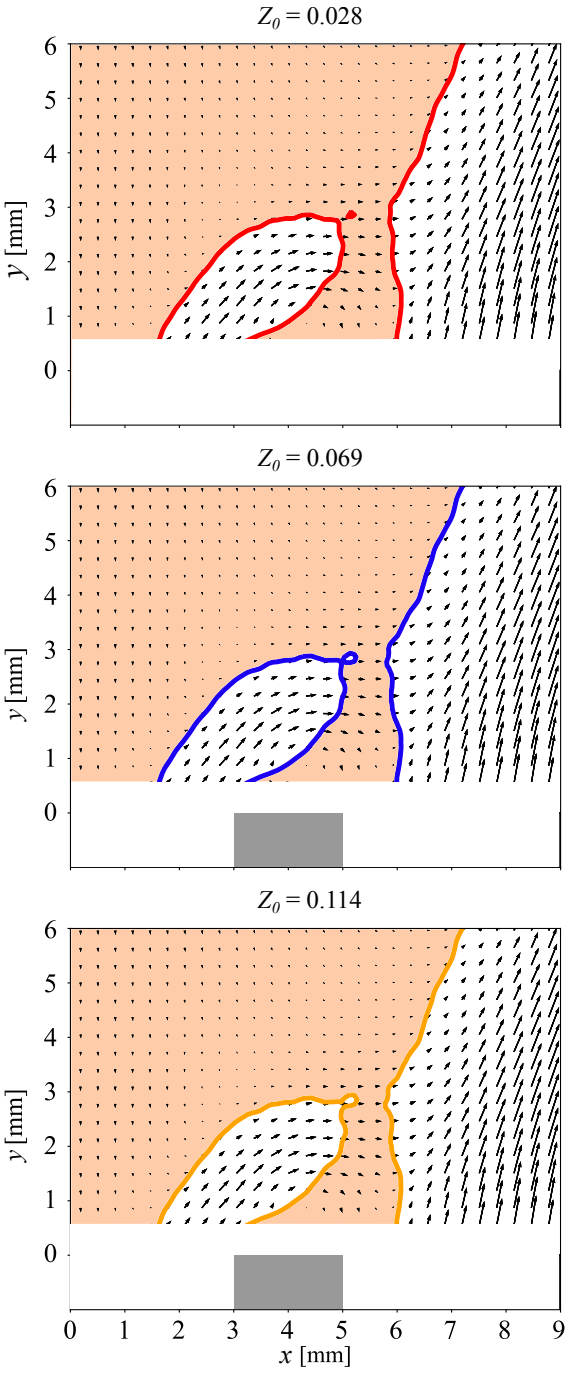

Figure 7: Sensitivity of the boundary of the TFUP zone (colored in orange) to the angle θ selected for the edge flame propagation line at Z_0. The operating conditions correspond to case $F_2 - 0.9 - Air/He$. The TFUP zone is drawn for the triple flame speed of H_2/air flame $s_d = 7.99$ m/s. PIV measurements realized in cold flow conditions.

the boundary of the TFUP zone is only slightly affected. Hence, in the following, only the angle θ deduced for $Z_0 = Z_{st} = 0.028$ is used to determine the boundary of the TFUP zone that has been shown to be a valid approximation.

Further measurements are made in cold flow conditions to determine the mixture fraction inside the TFUP zone with Raman scattering. Figure 8 shows the position of the stoichiometric mixture fraction $Z_0 = Z_{st} = 0.028$ deduced from Raman scattering at different heights above the burner when the central injector is fed with helium and with hydrogen. These data obtained in cold flow conditions are also compared with the detected flame front deduced from OH* images in Fig. 6 when the burner is powered by pure hydrogen. Conditions correspond to cases $F_2 - S_i - Air/He$ and $F_2 - S_i - Air/H_2$ featuring the same bulk injection velocities when the hydrogen flow is substituted by helium as for PIV measurements. This figure indicates that the location of the mixture fraction of helium $Y_{He} = 0.028$ determined in cold flow conditions matches well the location of the stoichiometric mixture fraction $Z_{st} = 0.028$ of the burner fed by hydrogen for all the swirl numbers $S_i = 0.0$ to $S_i = 0.9$ tested. It also confirms that the detected flame front used to determine the edge flame propagation line Z_0 well corresponds to the stoichiometric mixture fraction line Z_{st} deduced from Raman scattering in cold flow conditions for heights below 3 mm. Above 4 mm, the Z_{st} line in cold flow and the flame front begin to deviate from each other.

These tests indicate that helium can safely be used instead of hydrogen to determine the mixture fraction in the cold flow. This operation mode is preferred for obvious safety reasons. Moreover, it has been shown that the location of the stoichiometric line $Z_0 = 0.028$ measured by Raman scattering always lies near the flame front inferred from OH* images close to the hydrogen nozzle rim. In reacting conditions, the detected flame front is slightly shifted towards the external side due to thermal expansion in Fig. 8, which leads to a slightly higher angle θ with respect to the vertical axis. These small differences are however considered as acceptable and the angle θ of the edge flame propagation line is deduced in the following from OH* images.

The following method is finally used to determine the boundary of the TFUP zone for the different cases explored:

1. The angle θ between the edge flame propagation line Z_{st} and the vertical axis is first determined.
2. The velocity field in the axial plane of symmetry of the burner is determined with PIV in isother-

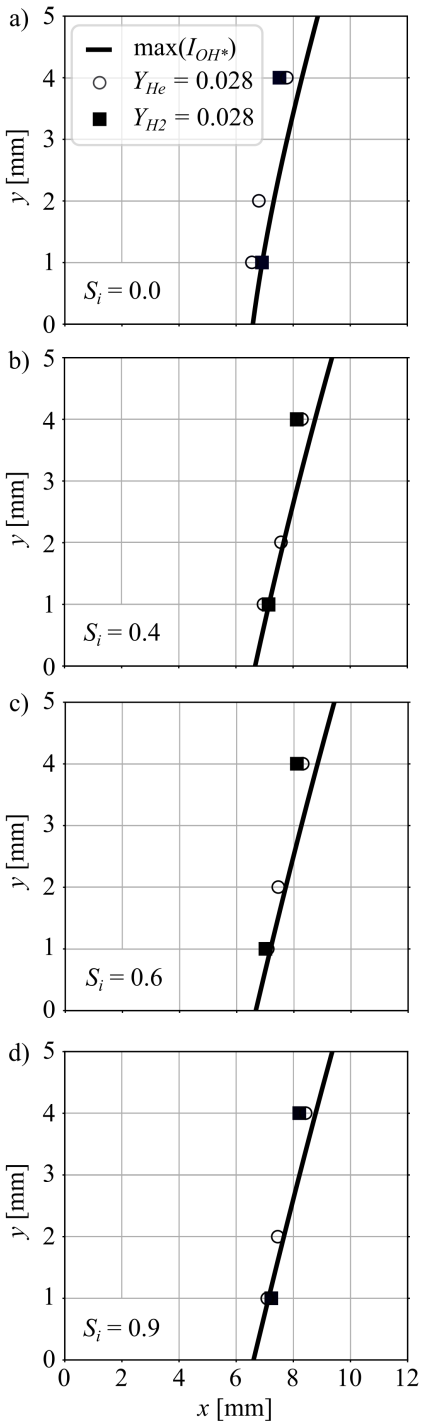

Figure 8: Comparison of the flame front location deduced from OH* images (reactive conditions) with the mixture fraction $Z = 0.028$ for H_2 and He swirled jets deduced from Raman scattering images (cold flow conditions). Cases $F_2 - S_i - Air/H_2$ and $F_2 - S_i - Air/He$ (see Table 1) with (a) $S_i = 0.0$, (b) $S_i = 0.4$, (c) $S_i = 0.6$ and (d) $S_i = 0.9$.

mal conditions with hydrogen being replaced by the same volumetric flowrate of helium.

3. The triple flame speed s_d is determined with Cantera and Eq. (2).
4. The boundary of the TFUP zone is deduced according to Eq. (4).

6. Validation of the TFUP model

Predictions from the TFUP model in cold flow conditions are now compared to observations of the flame stabilization regime when the inner swirl level S_i is varied. The case $F_2 - S_i - Air/He$ is again considered. The air bulk velocity is u_e = 28.5 m/s and the injection velocity in the central tube is u_i = 34 m/s. The inner swirl level is varied from S_i = 0.0 to S_i = 0.9. The colored lines in Fig. 9 correspond to the boundary of the TFUP zone on the air side where mixing between the pure hydrogen and air swirled jets takes place. The triple flame displacement speed used to draw this TFUP boundary is s_d = 7.99 m/s corresponding to the highest triple flame speed of H_2/air flames at ambient conditions. The markers identify to the location of the mixture fraction Z_m = 0.046 at y = 1 mm and 4 mm above the burner outlet that are deduced from Raman scattering measurements made in cold H_2/air flows. In all cases, the mixture fraction Z_m = 0.046 belongs to the TFUP zone. As a consequence, the edge flame velocity can be estimated with Eq. (2) for a mixture fraction Z_m = 0.046 yielding the maximum triple flame speed s_d of H_2/air flames. This consideration is further used below.

Figure 10 shows for cases $F_2 - S_i - Air/He$ how the velocity field and the boundary of the TFUP zone change for increasing values of the inner swirl level S_i (from top to bottom) and for decreasing values of the triple flame speed s_d (from left to right). The injection velocities are u_e = 28.5 m/s and u_i = 34 m/s. For the configuration without internal swirl S_i = 0.0 conferred to the central flow shown at the top in Fig. 10, the edge flame can always find a propagation path to the injector lips inside the TFUP when the triple flame speed changes from s_d = 6.0 m/s to 4.5 m/s. The predicted transition is only found by further reducing the triple flame speed to s_d = 1.2 m/s, a case which is not shown in this figure. In the absence of swirl conferred to the internal stream, very low flow velocities in the wake of the hydrogen injector rim foster flame anchoring to the injector.

In the second row in Fig. 10, the inner swirl number is slightly increased to S_i = 0.4. The swirl motion conferred to the internal stream produces a fast expansion

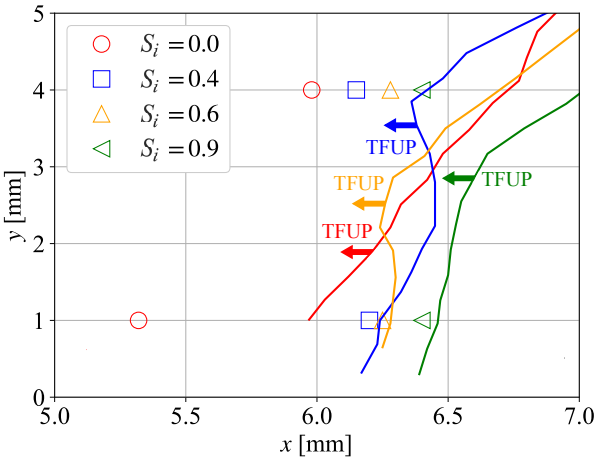

Figure 9: Comparison of the location of the mixture fraction Z_0 = 0.046 deduced from Raman scattering and corresponding to the highest laminar burning velocity s_d = 7.99 m/s of H_2/air flames at ambient conditions with the limit of the TFUP zone on the air side for the cases $F_2 - S_i - Air/He$ (Table 1) when the swirl S_i is varied.

of the central jet at the nozzle outlet and the TFUP zone in the wake of the central nozzle rim shrinks leaving only a small open channel for flame propagation when s_d = 6.0 m/s. The TFUP zone above the central injector lips is disrupted when s_d is further reduced between 5.5 m/s and 5.0 m/s. As a consequence, the minimum triple flame speed s_d at which flame re-anchoring is predicted greatly increases when the central stream is swirled. Here, the predicted minimum triple flame speed is s_d = 5.2 m/s for S_i = 0.4. This trend is exacerbated in the last two rows in Fig. 10 when the inner swirl number is further increased to S_i = 0.6 and S_i = 0.9. Transitions from lifted to re-anchored flames are predicted for minimum triple flame speed s_d = 5.6 m/s and s_d = 5.8 m/s respectively for S_i = 0.6 and S_i = 0.9.

To compare these predictions with the observed transitions, further experiments are carried out by modifying the gas composition inside the injection channels in order to control the value of the triple flame speed s_d and vary the boundary of the TFUP zone without altering the structure of the velocity field at the burner outlet. Change of the air composition inside the external channel is made by dilution with N_2. Inside the central channel, hydrogen is mixed with CH_4 and He. To limit perturbations of the velocity field, the injection velocities u_i and u_e and the total thermal power P are kept constant in these experiments.

Experiments are first conducted with hydrogen inside the central channel and air diluted by nitrogen inside the external channel. The burner is always ignited with

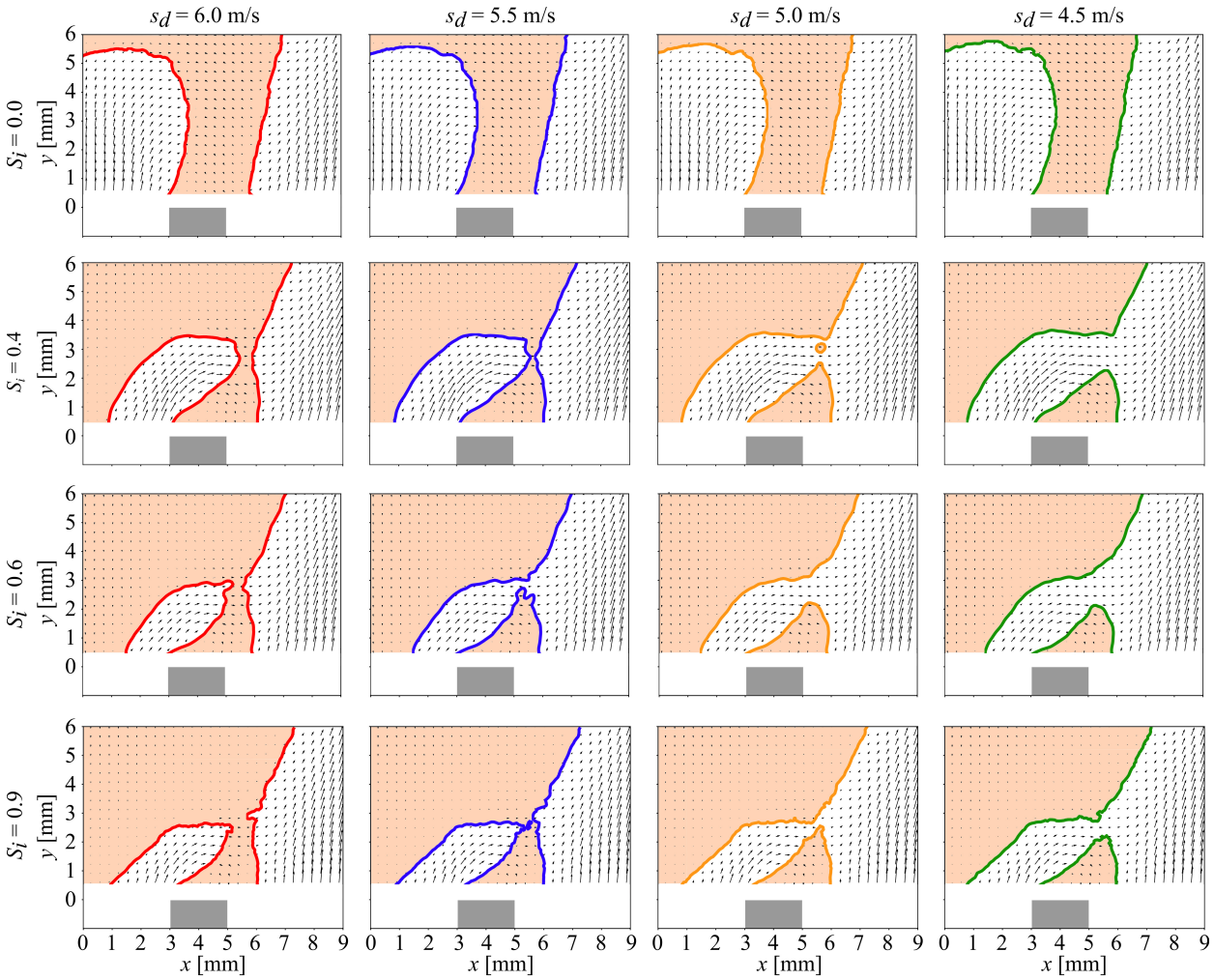

Figure 10: Evolution of the TFUP zone (colored in orange) with the selected triple flame displacement speed s_d deduced from PIV data taken in cold flow conditions. Operating conditions $F_2 - S_i - Air/He$ in Table 1. From top to bottom: S_i = 0.0, 0.4, 0.6 and 0.9.

Table 3: Evolution of the central jet angle α_i as a function of the gas composition Y_{H_2} and Y_{O_2} achieved with methane and helium in the central tube and nitrogen in the annular channel. The symbols for each observed transition correspond to those shown in Fig. 11. Operating conditions $F_2 - S_i - Air + N_2/H_2 + CH_4 + He$.

Case	$F_2-0.0$ $-Air+N_2/$ H_2+CH_4+He			$F_2-0.2$ $-Air+N_2/$ H_2+CH_4+He			$F_2-0.4$ $-Air+N_2/$ H_2+CH_4+He			$F_2-0.6$ $-Air+N_2/$ H_2+CH_4+He			$F_2-0.9$ $-Air+N_2/$ H_2+CH_4+He	
α_i [deg]	8			15			32			41			48	
Symbol	○	□	△	○	□	△	○	□	△	○	□	△	○	□
Y_{H_2}	0.28	0.15	0.08	0.54	0.43	0.31	1.00	0.87	0.77	1.00	0.87	0.77	1.00	0.77
Y_{O_2}	0.17	0.19	0.21	0.20	0.21	0.21	0.20	0.21	0.23	0.21	0.22	0.23	0.21	0.23

a high N_2 dilution rate in the external channel to reduce the value of the triple flame speed and start with a lifted flame. The nitrogen flowrate is then decreased step by step, in order to increase progressively the triple flame speed s_d until the flame re-anchors to the hydrogen nozzle rim. Nitrogen, air, and hydrogen flowrates

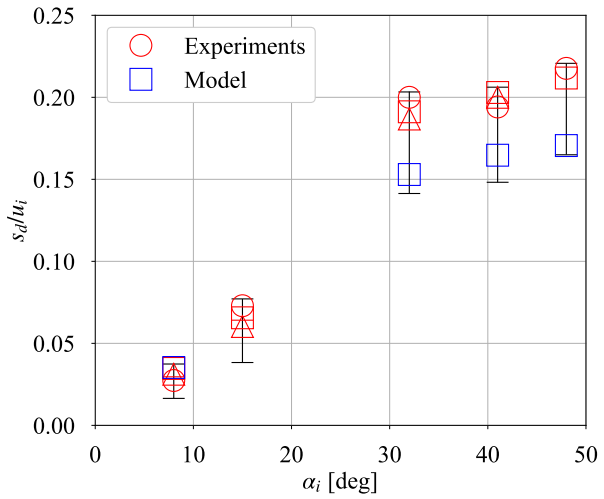

Figure 11: Comparison of the predicted flame transitions with experimental observations for cases $F_2 - S_i - Air + N_2/H_2 + CH_4 + He$ when the internal swirl level S_i changes from 0 to 0.9. Values for s_d are calculated with Cantera. The corresponding central jet angles α_i and the various compositions Y_{H_2} and Y_{O_2} are achieved with CH_4/He injected in the central tube and N_2 inside the annular channel as reported in Table 3.

at which this transition takes place are recorded and the corresponding value of the triple flame speed s_d is deduced from Cantera simulations. Experiments are then repeated by increasing the mass fraction of methane and helium in the central hydrogen channel. Experiments start again with a lifted flame and the flowrate of nitrogen is reduced until the flame re-anchors to the hydrogen nozzle.

Figure 11 compares the predicted transitions with observations for cases $F_2 - S_i - Air + N_2/H_2 + CH_4 + He$. The corresponding flow operating conditions are indicated in Table 1 and the gas compositions in Table 3. The normalized triple flame displacement speed s_d/u_i at which flame re-attachment takes place is plotted as a function of the expansion angle α_i of central jet. For fixed injection u_e and u_i velocities, α_i changes with the inner swirl number S_i as reported in Table 3. The square symbols in blue correspond to predictions of the TFUP model deduced from PIV data and a similar analysis as in Fig. 10. The red symbols denote conditions leading to the observed transition when the gas composition inside the internal and external channels are varied. The hydrogen Y_{H_2} and oxygen Y_{O_2} mass fractions are varied by injection of methane and helium in the central tube and nitrogen in the annular channel by keeping the injection velocities u_i and u_e constant. The values showing flame re-attachments are reported in Table 3. The corresponding uncertainty bars are drawn in Fig. 11. They mainly originate from the propagation of uncertainties on the flowrates used to deduce the triple flame speed s_d and the step width between operating points in both channels when the composition is changed.

Two important conclusions can be drawn from Fig. 11. For fixed flow injection conditions (u_i and u_e), the transition to flame re-anchoring is always found for the same value of the triple flame speed s_d regardless of the way the gas composition is changed inside of the external channel by dilution of air with nitrogen and regardless of the composition of the hydrogen mixture inside of the internal channel mixed with different concentrations of helium and methane. This proves that the edge flame speed is the correct physical parameter triggering these transitions for the range of operating conditions explored. Secondly, Fig. 11 also shows good agreement between predicted and observed transitions, with a small under estimation of the triple flame speed at which re-attachement takes place for the swirled cases when $S_i > 0$. Nevertheless, these differences remain small and within the error bars. Supplementary material is also provided with a similar figure as Fig. 11 to check the differences between experiments and predictions if one considers the laminar burning velocity s_l^0 instead of the triple flame displacement speed s_d. One may clearly identify in this supplementary material an offset by a factor of about 3 between the ratio s_l^0/u_i with respect to the transitions observed. These results nicely validate the TFUP model.

From a technological standpoint, it is more interesting to over predict the range where the flames are anchored than the opposite, because the lifted flames are the targeted ones in technical applications powered by hydrogen [9]. Figure 11 also highlights the benefits of swirling the hydrogen stream to enlarge the range of operating conditions with lifted flames [9, 14, 15]. Moreover, it can also be concluded that a moderate swirl number $S_i = 0.4$ already leads to a large widening of the burner operability with lifted flames. Increasing further the inner swirl number only produces a small improvement compared to operation with $S_i = 0.4$. The case for $S_i = 0.2$ is also reported in Fig. 11, but PIV data for the velocity field are not available for this case and as a consequence the TFUP zone could not be delimited.

The same experiments are now repeated for a fixed inner swirl level $S_i = 0.6$ varying the central injection velocity from $u_i = 17$ m/s to $u_i = 45$ m/s. This new set of experiments covers cases $F_1 - 0.6 - Air/He$, $F_2 - 0.6 - Air/He$ and $F_3 - 0.6 - Air/He$ for a fixed air injection velocity $u_e = 28.5$ m/s. The corresponding velocity fields in the wake of the central injector with the

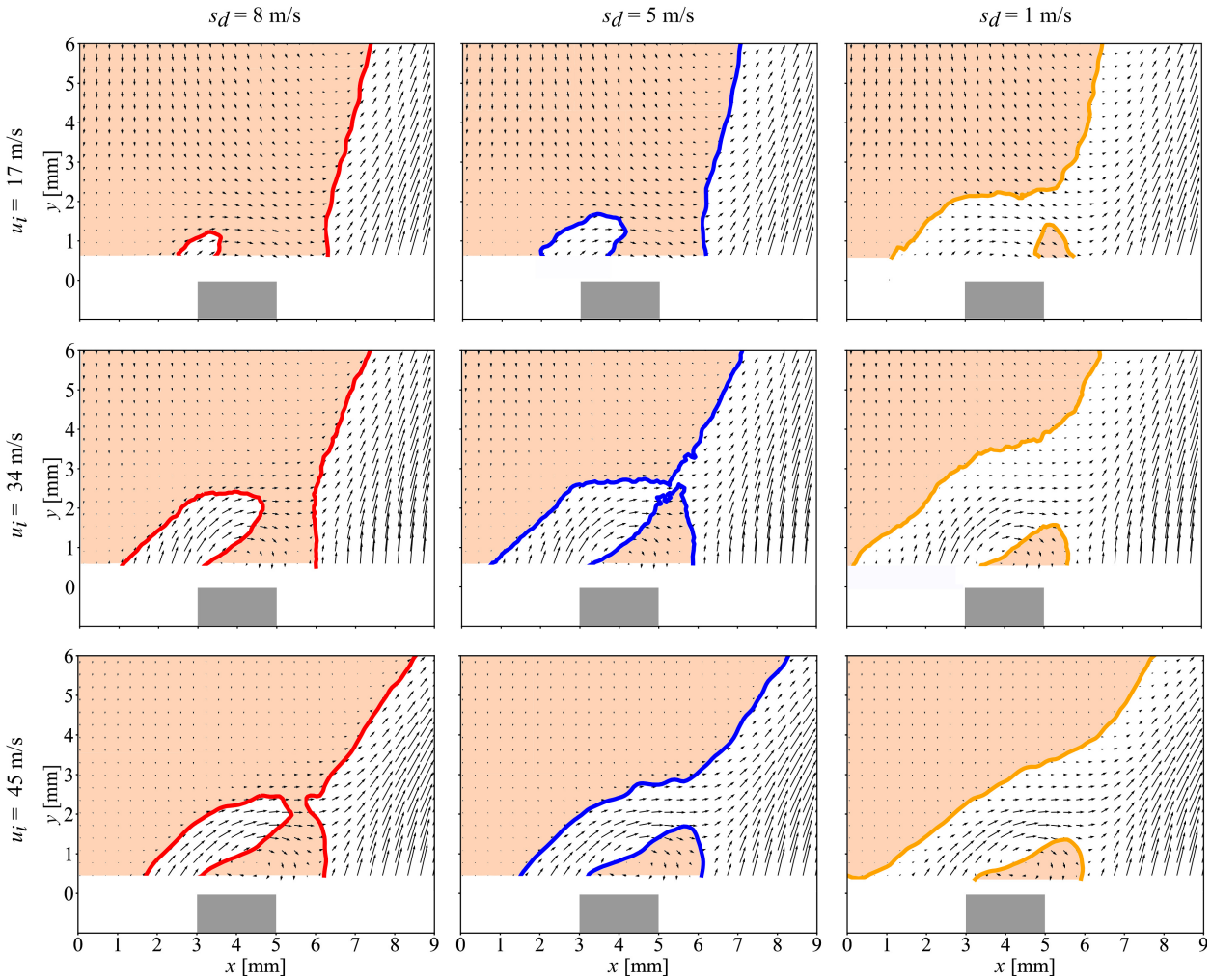

Figure 12: Evolution of the TFUP zone (colored in orange) deduced from PIV data with the triple flame displacement speed s_d for different central injection velocities u_i and a fixed inner swirl number $S_i = 0.6$. From top to bottom: u_i = 17, 34 and 45 m/s corresponding to cases $F_i - 0.6 - Air/He$ with $i = 1, 2$ and 3 (see Table 1).

Table 4: Evolution of the central jet angle α_i as a function of the gas composition Y_{H_2} and Y_{O_2} achieved with methane and helium in the central tube and nitrogen in the annular channel. The symbols for each observed transition correspond to those shown inFig. 13. Operating conditions $F_i - 0.6 - Air + N_2/H_2 + CH_4 + He$ with $i = 1, 2$ and 3.

Case	$F_1 - 0.6 - Air + N_2/H_2 + CH_4 + He$					$F_2 - 0.6 - Air + N_2/H_2 + CH_4 + He$			$F_3 - 0.6 - Air + N_2/H_2 + CH_4 + He$		
α_i [deg]	64					41			50		
Symbol	○	□	△	▷	◁	○	□	△	○	□	△
Y_{H_2}	1.00	0.77	0.60	0.48	0.39	1.00	0.87	0.77	1.00	0.87	0.77
Y_{O_2}	0.18	0.19	0.20	0.21	0.22	0.21	0.22	0.23	0.22	0.23	0.23

TFUP boundaries superimposed are presented in Fig. 12 for different values of the triple flame speed s_d. In the top row in Fig. 12 obtained for the lowest central injection velocity u_i = 17 m/s with $\alpha_i = 64°$ (see Table 4), the velocity in the wake of the hydrogen injector lips remains low because of the low impulsion of the central

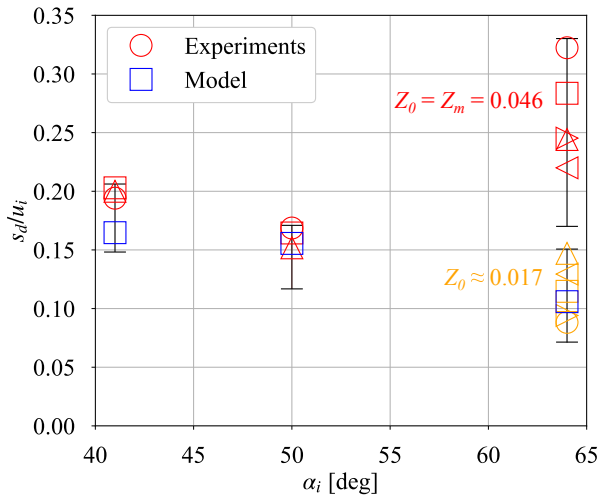

Figure 13: Comparison of the predicted flame transitions with observations made for cases $F_i - 0.6 - Air + N_2/H_2 + CH_4 + He$ with $i = 1, 2$ and 3 when the internal velocity u_i changes from 17 to 45 m/s (see Tables 1 and 4). Orange symbols correspond to s_d values calculated at the highest equivalence ratio measured in the TFUP zone. Red symbols correspond to s_d values calculated for the maximum laminar burning velocity.

jet. This leads to a very small velocity projected in the reference frame of the edge flame and to a small value of the predicted triple flame speed $s_d = 1.8$ m/s above which the flame reattaches. Coherently, this threshold level is comparable to the one $s_d = 1.2$ m/s obtained for the non-swirling central jet case $S_i = 0.0$ in Fig. 10. Results in the second row in Fig. 12 coincide with the third row in Fig. 10 obtained for $S_i = 0.6$, $u_i = 34$ m/s leading to $\alpha_i = 41°$ (Table 4) and were already commented. In this case, the predicted minimum triple flame speed leading to flame re-attachment is $s_d = 5.6$ m/s. Finally, the bottom row shows the case with the highest central injection velocity $u_i = 45$ m/s in which case $\alpha_i = 50°$ (Table 4). For this last case, the velocities above the central injector lips take much higher values. Flame re-anchoring is hindered in this region characterized by high velocities and transition to anchored flame would require values of the triple flame speed higher than $s_d = 7.0$ m/s. These results confirm previous observations made in [9, 10]. For a fixed dual swirl injector geometry and a fixed gas composition, i.e. a fixed value of s_d, the injection velocity u_i of the fuel in the central tube is the main parameter determining the flame stabilization regime for the range of operating conditions explored.

Predictions deduced from Fig. 12 in cold flow conditions are compared in Fig. 13 to the observations made for the flame stabilization regime for cases $F_i - 0.6 - Air + N_2 - H_2 + CH_4 + He$ with $i = 1, 2, 3$ for a fixed internal swirl level $S_i = 0.6$ (see Tables 1 and 4). As in Fig. 11, results are presented for the ratio s_d/u_i as a function of the expansion angle α_i of the central jet. Values for α_i, Y_{H_2} and Y_{O_2} are reported in Table 4. This figure highlights two important features.

For $\alpha_i = 41^o$ and 50^o, the value of the triple flame speed s_d used for the prediction of the transition is deduced with Eq. (2) from the combustible mixture featuring the highest laminar burning velocity and it has been checked with Raman scattering that this mixture fraction is effectively reached by the flow within the TFUP zone. In these cases, the predictions in blue match well with the transitions that are observed. However for the last operating condition, corresponding to $\alpha_i = 64^o$ obtained for the lowest injection velocity $u_i = 17$ m/s, the equivalence ratio in the TFUP zone measured by Raman scattering does not exceed $\phi \simeq 0.6$ for H_2/air flames. In this latter case, the mixture fraction $Z_m = 0.046$ leading to the highest laminar burning velocity does not belong to the TFUP zone and the edge flame can only propagate along the highest mixture fraction which is available in the TFUP zone. For this last operating condition, predictions are presented in Fig. 13 in red for s_d calculated with $Z_m = 0.046$ corresponding to the highest laminar burning velocity of the combustible mixture. They are also plotted for $Z_0 = 0.017$ (for H_2/air flames) corresponding to the maximum mixture fraction that has been measured inside the TFUP zone at $y = 4$ mm by Raman scattering. The TFUP model over-estimates the threshold ratio s_d/u_i below which the flame re-anchors with $Z_m = 0.046$. Predictions match better the observed transition with the measured mixture fraction $Z_0 = 0.017$.

A similar atypical behavior has already been observed in a previous study carried out for non-swirling jet flames with a small co-flow. This last regime was identified as a premixed propagation regime in [36]. In this regime, the edge flame velocity cannot be estimated with the triple flame speed calculated at the equivalence ratio corresponding to the maximum laminar burning velocity. A good estimation can however be obtained by determining the laminar burning velocity with Eq. (2) at the highest equivalence ratio available for the edge flame in the TFUP zone. Here, the maximum mixture fraction available for the edge flame is $Z_0 = 0.017$ corresponding to an equivalence ratio $\phi \simeq 0.6$ for H_2/air flames.

It is worth recalling that all results that were presented in this study were obtained with two-dimensional PIV measurements and one dimensional Raman scattering measurements made in cold flow conditions. The

effect of swirl on the flow velocity field is taken into account by considering the radial component of the velocity field. This has been shown to be sufficient to predict transitions from lifted to re-anchored flames when the inner swirl level, the central injection velocity, and the composition of the reactants inside the external and internal channels are modified. The impact of the three dimensional structure of the flow has been discarded in this study and several approximations have been made to deduce the edge flame propagation trajectory based on an analysis of the mean velocity field and the mean composition of the fuel and oxidizer swirled flow. Moreover, the impact of thermal expansion through the flame has also been discarded. The impact of gas pre-heating by thermal conduction through solid components and heat-losses have also been neglected. Nonetheless, it has been shown that the TFUP model always yields results very close to the transitions observed. Finally, it is also worth mentioning that the companion problem of the transition from anchored to lifted flames is not considered in this paper. Initial experiments indicate that the physical mechanisms leading to flame detachment are different than those controlling flame re-anchoring.

7. Conclusion

The stabilization regime of partially premixed H_2/air flames stabilized above a dual-swirl coaxial injector has been investigated. A predictive model called TFUP for Triple Flame Upstream Propagation has been improved and validated with detailed flow characterizations. It has been shown that:

- Mixing between the inner swirled hydrogen jet and the outer swirled air jet in a dual swirl coaxial injector can be investigated by substituing helium instead of hydrogen in cold flow conditions to determine the mixture fraction.
- The TFUP model based on PIV data and mixture fraction measurements made in cold flow conditions yields satisfactory predictions of the transition from lifted to re-anchored flames when the inner swirl, the central injection velocity, and the gas composition in the internal and external injection channels are varied.
- In a dual coaxial swirl hydrogen injector, the large enhancement of the operability range with lifted flames when swirl is conferred to the central hydrogen stream has been elucidated and is attributed to the fast expansion of the central jet cutting the low velocity zone above the hydrogen injector lips.
- In most cases, the TFUP model can be applied without knowledge of the exact mixture composition inside the TFUP zone by considering that an edge flame will propagate at the triple flame speed of a combustible mixture formed by the fuel and oxidizer featuring the maximum laminar burning velocity. When the combustible mixture remains lean in the TFUP zone, the edge flame propagates along the line with the highest equivalence ratio and at the triple flame speed determined for this equivalence ratio. In all cases, the predicted transition from lifted to anchored flame is in good agreement with experimental observations.

Future experiments will aim at further analyzing the impact of the outer swirl level, the inner and outer diameters of the dual swirl coaxial injector, and the thickness of the injector lips. The TFUP model needs also to be validated for increased pressure and temperature of inlet gases, which is not possible to achieve with the current test bench. The TFUP model however paves the way to design burners with separate injections of hydrogen and air resulting in lifted flames. Indeed, the model can be used from numerical flow simulations in cold flow conditions for preliminar design of combustors, or from a reference operating point with certain assumptions on the evolution of the flow field when parameters, as injection temperature and pressure for example, are varied.

Acknowledgements

This project has received funding from the European Research Council under the European Union's Horizon 2020 research and innovation program Grant Agreement 832248, SCIROCCO and under the Horizon 2020, COEC (Center of Excellence in Combustion) program, Grant Agreement 952181. The authors are grateful to the technical support from G. Albert, S. Cazin, S. Lun Kwong Leon, M. Marchal, L. Mouneix and R. Soeparno from IMFT.

References

[1] G. Kakoulaki, I. Kougias, N. Taylor, F. Dolci, J. Moya, A. Jäger-Waldau, Green hydrogen in europe – a regional assessment: Substituting existing production with electrolysis powered by renewables, Energ. Convers. Manage. 228 (2021) 113649.
[2] Clean sky 2, https://www.clean-aviation.eu/clean-sky-2 (2021).
[3] P. Chiesa, G. Lozza, L. Mazzocchi, Using hydrogen as gas turbine fuel, J. Eng. Gas Turb. Power 127 (2005) 73–80.

[4] G. Richards, M. McMillian, R. Gemmen, W. Rogers, S. Cully, Issues for low-emission, fuel-flexible power systems, Prog. Energ. Combust. 27 (2001) 141–169.

[5] O. Tuncer, S. Acharya, J. Uhm, Dynamics, NOx and flashback characteristics of confined premixed hydrogen-enriched methane flames, Int. J. Hydrogen Energ 34 (2009) 496–506.

[6] C. Eichler, G. Baumgartner, T. Sattelmayer, Experimental investigation of turbulent boundary layer flashback limits for premixed hydrogen-air flames confined in ducts, J. Eng. Gas Turb. Power 134 (2011) 011502.

[7] R. W. Schefer, T. D. Slith, C. J. Marek, Evaluation of NASA lean premixed hydrogen burner, Tech. rep., Sandia National Laboratories (2003).

[8] H. H.-W. Funke, N. Beckmann, J. Keinz, A. Horikawa, 30 Years of dry-low-NOx micromix combustor research for hydrogen-rich fuels—An overview of past and present activities, J. Eng. Gas Turb. Power 143 (2021) 071002.

[9] S. Marragou, H. Magnes, T. Poinsot, L. Selle, T. Schuller, Stabilization regimes and pollutant emissions from a dual fuel CH4/H2 and dual swirl low NOx burner, Int. J. Hydrogen Energ 47 (2022) 19275–19288.

[10] S. Marragou, H. Magnes, A. Aniello, L. Selle, T. Poinsot, T. Schuller, Experimental analysis and theoretical lift-off criterion for H2/air flames stabilized on a dual swirl injector, P. Combust. Inst. In Press.

[11] N. Syred, J. Beér, Combustion in swirling flows: A review, Combust. Flame 23 (1974) 143–201.

[12] A. Degenève, R. Vicquelin, C. Mirat, B. Labegorre, P. Jourdaine, J. Caudal, T. Schuller, Scaling relations for the length of coaxial oxy-flames with and without swirl, P. Combust. Inst. 37 (2019) 4563–4570.

[13] D. Laera, P. Agostinelli, L. Selle, Q. Cazères, G. Oztarlik, T. Schuller, L. Gicquel, T. Poinsot, Stabilization mechanisms of CH4 premixed swirled flame enriched with a non-premixed hydrogen injection, P. Combust. Inst. 38 (2021) 6355–6363.

[14] S. Yuasa, Effects of swirl on the stability of jet diffusion flames, Combust. Flame 66 (1986) 181–192.

[15] A. Degeneve, C. Mirat, J. Caudal, R. Vicquelin, T. Schuller, Effects of swirl on the stabilization of non-premixed oxygen-enriched flames above coaxial injectors, J. Eng. Gas Turb. Power 141.

[16] A. Degeneve, R. Vicquelin, C. Mirat, J. Caudal, T. Schuller, Impact of co- and counter-swirl on flow recirculation and liftoff of non-premixed oxy-flames above coaxial injectors, P. Combust. Inst. 38 (2021) 5501–5508.

[17] M. Leroy, C. Mirat, A. Renaud, R. Vicquelin, Stabilization of low-NOx hydrogen flames on a dual-swirl coaxial injector, J. Eng. Gas Turb. Power 145 (2022) 021021.

[18] A. Katoch, T. F. Guiberti, D. V. de Campos, D. A. Lacoste, Dual-fuel, dual-swirl burner for the mitigation of thermoacoustic instabilities in turbulent ammonia-hydrogen flames, Combust. Flame 246 (2022) 112392.

[19] A.-H. Chen, J. F. Driscoll, J. Kelly, M. Namazian, R. W. Schefer, A comparison of bluff-body and swirl stabilized flames, Combust. Sci. Technol. 71 (1990) 197–217.

[20] S. Kim, J. Yoon, Y. Yoon, Internal flow characteristics of liquid-liquid swirl coaxial injectors with different recess lenghts and oxidizer-fuel ratios, Atomization Spray 21 (2011) 971–987.

[21] S. Silvestri, M. P. Celano, C. Kirchberger, G. Schlieben, O. Haidn, O. Knab, Investigation on recess variation of a shear coax injector for a single element GOX-GCH4 combustion chamber, T. Jpn. Soc. Aeronaut. S. 14 (2016) 13–20.

[22] W. M. Pitts, Assessment of theories for the behavior and blowout of lifted turbulent jet diffusion flames, Symposium (Int.) Combust. 22 (1989) 809–816.

[23] L. Vanquickenborne, A. van Tiggelen, The stabilization mechanism of lifted diffusion flames, Combust. Flame 10 (1966) 59–69.

[24] N. Peters, F. A. Williams, Liftoff characteristics of turbulent jet diffusion flames, AIAA J. 21 (1983) 423–429.

[25] S. Byggstoyl, B. F. Magnussen, A model for flame extinction in turbulent flow, Turbul. Shear Flows 4 (1984) 381–395.

[26] H. Im, J. Chen, Structure and propagation of triple flames in partially premixed hydrogen–air mixtures, Combust. Flame 119 (1999) 436–454.

[27] R. Schefer, M. Namazian, J. Kelly, Stabilization of lifted turbulent-jet flames, Combust. Flame 99 (1994) 75–86.

[28] J. Buckmaster, Edge-flames, Prog. Energ. Combust. 28 (2002) 435–475.

[29] M. S. Cha, P. D. Ronney, Propagation rates of nonpremixed edge flames, Combust. Flame 146 (2006) 312–328.

[30] D. B. Clayton, M. S. Cha, P. D. Ronney, Propagation and extinction of premixed edge-flames, P. Combust. Inst. 37 (2019) 1823–1830.

[31] L. Muñiz, M. Mungal, Instantaneous flame-stabilization velocities in lifted-jet diffusion flames, Combust. Flame 111 (1997) 16–31.

[32] G. R. Ruetsch, L. Vervisch, A. Liñán, Effects of heat release on triple flames, Phys. Fluids 7 (1995) 1447–1454.

[33] T. C. Lieuwen, Unsteady Combustor Physics, Cambridge University Press, 2012. doi:10.1017/CBO9781139059961.

[34] C. D. Brown, K. A. Watson, K. M. Lyons, Studies on lifted jet flames in coflow: the stabilization mechanisms in the near- and far-fields, Flow Turbul. Combust. 62 (1999) 249–273.

[35] A. Joedicke, N. Peters, M. Mansour, The stabilization mechanism and structure of turbulent hydrocarbon lifted flames, P. Combust. Inst. 30 (2005) 901–909.

[36] T. F. Guiberti, W. R. Boyette, Y. Krishna, W. L. Roberts, A. R. Masri, G. Magnotti, Assessment of the stabilization mechanisms of turbulent lifted jet flames at elevated pressure using combined 2-D diagnostics, Combust. Flame 214 (2020) 323–335.

[37] G. Oztarlik, L. Selle, T. Poinsot, T. Schuller, Suppression of instabilities of swirled premixed flames with minimal secondary hydrogen injection, Combust. Flame 214 (2020) 266–276.

[38] R. Price, I. Hurle, T. Sugden, The filtered abel transform and its application in combustion diagnostics, Symposium (Int.) Combust. 12 (1969) 1093–1102.

[39] A. Aniello, D. Laera, S. Marragou, H. Magnes, L. Selle, T. Schuller, T. Poinsot, Experimental and numerical investigation of two flame stabilization regimes observed in a dual swirl H2-air coaxial injector, Combust. Flame In press.

[40] R. Schefer, W. Kulatilaka, B. Patterson, T. Settersten, Visible emission of hydrogen flames, Combust. Flame 156 (2009) 1234–1241.

[41] T. Fiala, T. Sattelmayer, Heat release and UV–Vis radiation in non-premixed hydrogen–oxygen flames, Exp. Fluids. 56 (2015) 1–15.

[42] C. W. Foley, I. Chterev, J. Seitzman, T. Lieuwen, High resolution particle image velocimetry and CH-PLIF measurements and analysis of a shear layer stabilized flame, J. Eng. Gas Turbine Power 138 (3).

[43] Mechanical, A. E. C. Research, Chemical-kinetic mechanisms for combustion applications (2012).
URL `http://combustion.ucsd/edu`